ELSEVIER

Journal of Structural Geology 27 (2005) 419–431

JOURNAL OF STRUCTURAL GEOLOGY

www.elsevier.com/locate/jsg

Does cation ordering in omphacite influence development of lattice-preferred orientation?

Stanislav Ulrich[a,b,*], David Mainprice[c]

[a]*Institute of Geophysics, Czech Academy of Sciences, Boční II/1401, 14131 Praha 4, Czech Republic*
[b]*Institute of Petrology and Structural Geology, Charles University, Albertov 6, 12843 Praha 2, Czech Republic*
[c]*Laboratoire de Tectonophysique, ISTEEM, Université de Montpellier II, Pl. E. Bataillon, 34095 Montpellier, France*

Received 14 April 2004; received in revised form 29 October 2004; accepted 8 November 2004
Available online 25 January 2005

Abstract

Three mantle eclogite xenoliths from the Robert Victor mine in South Africa were studied. The calculated *pT* conditions are $p \geqq 4.5$ GPa and *T* between 950 and 1145 °C. The clinopyroxene has a jadeite component between 0.19 and 0.52. In-situ, at these compositions and temperatures clinopyroxene (omphacite) has the high temperature C2/c structure, which has perfect cation disordering. The lattice preferred orientation (LPO) of clinopyroxene in the samples of different microstructure and composition has been measured by EBSD. The LPO for all three samples is characterized by a strong alignment of the [001] axes with the lineation, typical of the 'L-type' or 'LS-type' patterns for omphacite. These data disagree with a cation-ordering model for dislocation slip, which predicts a 'S-type' LPO pattern with the [001] axes forming a girdle in the foliation plane. Numerical simulation using the VPSC model has been undertaken to show the influence of the $\langle 110\rangle\{1\bar{1}0\}$ slip system on the LPO development in axially symmetric compression and extension, and pure and simple shear. The activity of the $\langle 110\rangle\{1\bar{1}0\}$ system should be very sensitive to changes in the cation ordering as the clinopyroxene goes towards the low temperature fully ordered P2/n structure. Increasing the critical resolved shear stress on this system from 1 to 10, resulted in a decrease of the slip activity of 80%, but produced no significant changes to the LPO. The most important slip systems for LPO development are [001](100), [100](010) and [001](010) in all simulations. The LS-index is introduced to quantify the symmetry of omphacite LPO. The index is based on the eigenvalues of the (010) and [001] pole figures, and has a value of one for the end-member L-type, zero for the end-member S-type and intermediate values for LS-types. The naturally deformed omphacite LPOs have LS-indexes of between 0.61 and 0.85 confirming they are LS-types, but closer to the L-type end-member. In the VPSC models the S-type end-member develops in axially symmetric compression (LS-index ≈ 0), whereas the L-type end-member develops in axially symmetric extension (LS-index ≈ 1). In simple and pure shear the LS-type fabric develops with LS-index of between 0.55 and 0.60. The VPSC simulations show that the LS-index is nearly constant with increasing strain for a constant macroscopic velocity gradient, which prescribes the constant strain path. We conclude that development of S- and L-type LPOs in omphacite is controlled by the strain path and that the LS-index is a useful quantitative indicator of fabric symmetry.

Keywords: Clinopyroxene; Lattice-preferred orientation; Strain; Cation-ordering; Mantle eclogite

1. Introduction

Clinopyroxene, namely diopside and omphacite, have been the subject of various experimental studies due to their high abundance in eclogite, mafic and ultramafic rock types. Experimental work on diopside (C2/c space group) single crystals and aggregates show that there are several glide systems reported with dominant [001](100) (Kirby and Christie, 1977; Avé Lallemant, 1978; Kollé and Blacic, 1983; Kirby and Kronenberg, 1984), but also $1/2\langle 110\rangle\{1\bar{1}0\}$, $1/2\langle 110\rangle(001)$, [001](010), $[201](\bar{1}02)$ (Avé Lallemant, 1978) and lamellar features parallel to (101) that could be microtwins or slip bands (Kirby and Christie, 1977). Ratteron et al. (1994) found predominance of [001](100) slip system between 800 and 1000 °C, whereas $1/2\langle 110\rangle\{1\bar{1}0\}$ becomes more important above 1000 °C in the diopside single crystals.

* Corresponding author. Correspondence address: Institute of Geophysics, Czech Academy of Sciences, Boční II/1401, 14131 Praha 4, Czech Republic. Tel.: +420-267103017; fax: +420-272761549
E-mail address: stano@ig.cas.cz (S. Ulrich).

0191-8141/$ - see front matter © 2005 Elsevier Ltd. All rights reserved.
doi:10.1016/j.jsg.2004.11.003

Study of clinopyroxene (omphacite, either C2/c or P2/n space groups) lattice preferred orientation (LPO) in naturally deformed eclogites showed that there are L- and S-types of texture (Helmstaedt et al., 1972). The L-type is characterized by [001] axes, which lie preferentially parallel to the lineation and (010) poles in the plane normal to the lineation, whereas S-type shows [001] axes form a girdle in the foliation plane and (010) planes are parallel to the foliation. More recent measurements showed that omphacite develops various transitional types between L- and S-types of LPO suggesting activity of [001]{110}, [001](100) and 1/2⟨110⟩{1$\bar{1}$0}, slip systems (e.g. Van Roermund and Boland, 1981; Van Roermund, 1983; Godard and Van Roermund, 1995; Mauler et al., 1998, 2000, 2001; Bascou et al., 2001) which we will call LS-type.

Naturally deformed omphacite is composed of disordered (space group C2/c) solid solution, onto which a cation ordering (P2/n) is superimposed (e.g. Carpenter, 1979, 1983). Experiments have shown that a thermodynamically continuous transition line (C2/c–P2/n), peaking at ca. 865 °C (augite–jadeite system) and ca. 750 °C (diopside–jadeite system), and miscibility gaps between the C2/c and P2/n fields at lower temperatures in the binary equilibrium phase versus temperature diagram (e.g. Carpenter, 1983; Davidson and Burton, 1987). Brenker et al. (2002) presented microstructural and LPO data of omphacite from a suite of eclogites from the Adula/Cima Lunga nappe (Central Alps) together with previously published LPO of omphacite and concluded that cation ordering in omphacite controls development of either L-type LPO (ordered structure) or S-type LPO (disordered structure). They argued that the perfect dislocation of Burgers vector $\mathbf{b}=1/2\langle 110\rangle$, in the disordered high temperature structure (C2/c) transforms to $\mathbf{b}=\langle 110\rangle$ of unit translation in the low temperature ordered structure (P2/n). To reduce energy the $\mathbf{b}=\langle 110\rangle$, dislocation dissociates into two partials separated by a stacking fault in the structure (P2/n). Brenker et al. (2002) argued that the difference in dislocation structure for the ⟨110⟩ slip direction changes the relative ease of slip in the ⟨110⟩ and [001] directions for the high (C2/c) and low (P2/n) temperature structures, which in turn gives rise to different LPOs. Finally, the authors considered that the degree of cation ordering is the prime control on the development of LPO in omphacite, with S-type occurring at higher temperature in the stability field of C2/c and L-type occurring at lower temperature in the stability field of P2/n.

In this work, we present L-type LPO of naturally deformed omphacite from the eclogite nodules brought to the surface by kimberlite eruptions in the Kaapvaal craton, South Africa. All nodules are from the Roberts Victor mine, which is well known for the high abundance of mantle eclogites (Hatton and Gurney, 1978). The previous temperature estimates for eclogites from the Roberts Victor mine show that they equilibrated between 950 and 1150 °C (Carswell et al., 1981) and have been part of the craton since Archean times (Shirey et al., 2001) until their rapid exhumation to the surface during the Cretaceous kimberlite eruptions. Yokoyama et al. (1976) have shown that the omphacite in these mantle eclogites have a completely disordered structure and following conclusions of Brenker et al. (2002), omphacite should have a characteristic S-type LPO. Finally, numerical calculation of LPO has been carried out using a visco-plastic self-consistent (VPSC) model in order to verify the effect of slip activity of ⟨110⟩{1$\bar{1}$0} on LPO formation.

2. Description of the samples

The xenoliths HRV277 and HRV113 were sampled in the Roberts Victor kimberlite pipe and FRB1300 in the Premier Mine, all located in the archean Kaapvaal craton, South Africa. Sample HRV277 is a coesite + kyanite + sanidine eclogite of coarse-grained microstructure with slightly elongated garnets (1–3 mm in size) defining foliation together with kyanite (Fig. 1a). In the thin section, all the mentioned minerals and their grain boundaries are well preserved except clinopyroxene, which is strongly altered. Coesite grains show rims of polycrystalline quartz. The other two samples are bimineralic eclogites having a different microstructure. Original grain boundaries are altered and hardly defined. The sample HRV113 shows a coarse-grained microstructure with homogenous spatial distribution of rounded garnet grains (4–8 mm in diameter) surrounded by clinopyroxene (Fig. 1b). The sample HRV1300 shows solid-state deformation fabric with foliation defined by regular distribution of elongated garnet crystals (3–6 mm length) and coarse-grained clinopyroxene (Fig. 1c).

3. Methods

3.1. Chemical analysis and equilibration temperature

Electron microprobe point analyses of original mantle minerals, namely clinopyroxene and garnet, have been conducted with a Cameca SX 100 in Montpellier and in the same type of microprobe in Prague. Data from neighboring grains have been used to calculate equilibration temperature, which is estimated from the empirical relationship between Ca-content in garnet and Fe^{2+}–Mg^{2+} partitioning between coexisting garnets and clinopyroxenes (Ellis and Green, 1979; Powell, 1985; Ai, 1994). Unfortunately, there is no reliable geobarometer for this mineral association, but mantle eclogites can be classified into diamond-bearing Group I or diamond-free Group II according to K_2O_{cpx} and Na_2O_{grt} content (McCandless and Gurney, 1989). Eclogites with average $K_2O_{cpx} \geqq 0.08$ wt% or $Na_2O_{grt} \geqq 0.09$ wt% are considered to be Group I, and eclogites with levels below these form Group II. As the detection limits of the microprobes for amount of K_2O_{cpx} (0.02 wt%) and Na_2O_{grt} (0.03 wt%) are small enough to assign eclogites either to

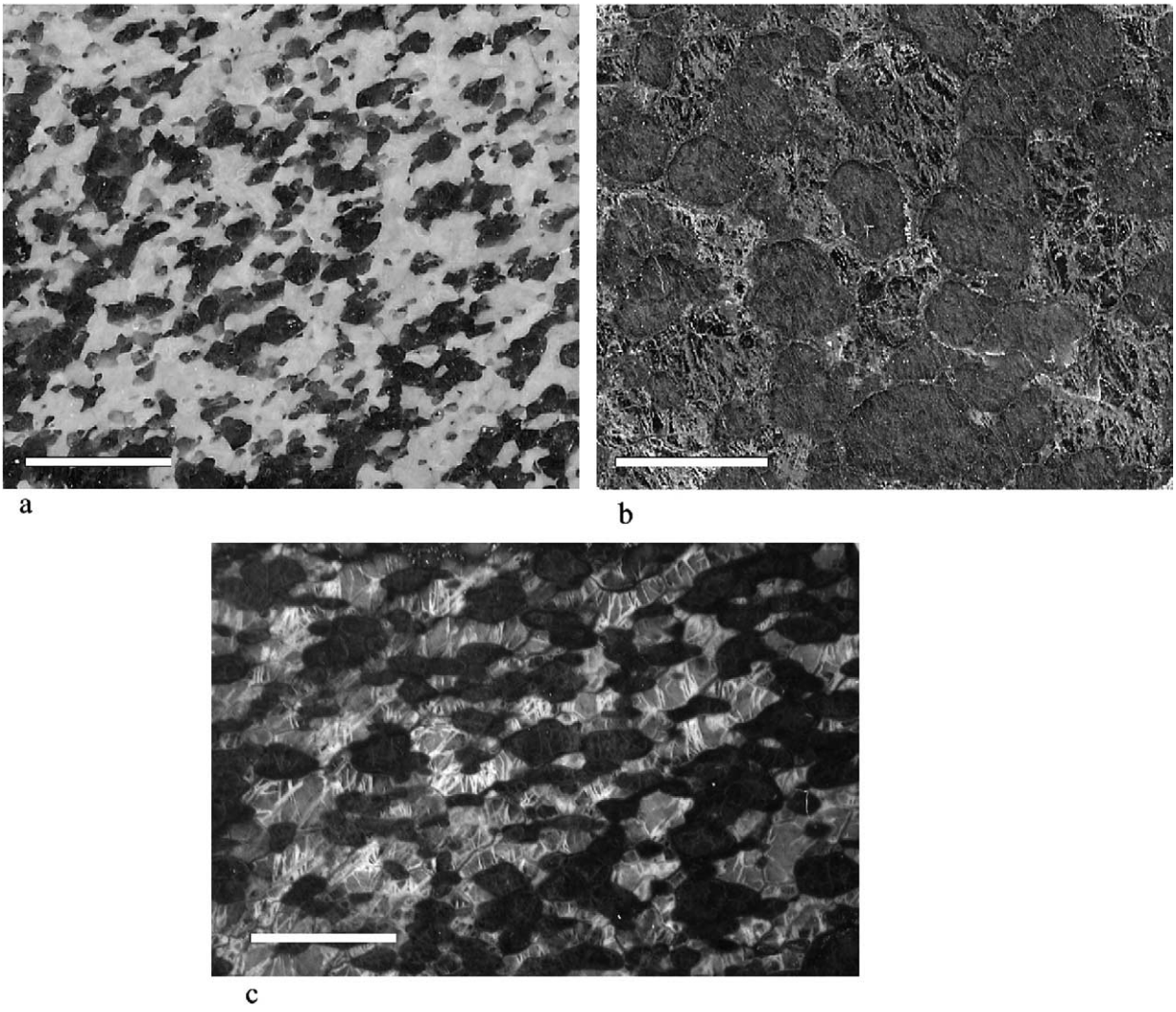

Fig. 1. Microphotos of studied samples. (a) A sample HRV277. Black elongated crystals are garnets defining foliation plane. White groundmass is strongly altered clinopyroxene. Dark and light gray minerals are kyanite and sanidine, and coesite, respectively. (b) A sample HRV113. Round-shaped crystals of dark gray color are garnets surrounded by large crystals of altered clinopyroxenes. (c) A sample FRB1300. Dark elongated crystals are garnets surrounded by partially altered clinopyroxenes of light gray color. Length of the white bar in the bottom left is 1.0 cm.

Group I or Group II, a pressure could be roughly estimated for the equilibration temperature. Finding the intersection of the graphite–diamond phase boundary (Kennedy and Kennedy, 1976) with the model conductive geotherm for Kaapvaal craton (Pollack and Chapman, 1977; Ryan et al., 1996; Viljoen, 1999), values of 4 and 4.5 GPa were estimated to correspond to the maximum equilibration temperature for Group II eclogites and the minimum equilibration temperature for Group I eclogites, respectively. Additionally, composition profiles through garnet and clinopyroxene were measured in order to study their chemical homogeneity (Fig. 2).

3.2. Lattice preferred orientation

Omphacite LPOs were measured on a scanning electron microscope CamScan4 in Prague and Jeol5600 in Montpellier by electron backscattered diffraction (EBSD; Adams et al., 1993) using HKL technologies CHANNEL 5 software (Schmidt and Olesen, 1989). In order to improve the quality of the diffraction patterns a SYTON chemical polishing minimized the surface topography of the samples. A light carbon coating and using an accelerating voltage of 17 kV reduced electrical charging effects. Diffraction patterns were acquired at a working distance of about 40 mm, which permitted the study of large polished surfaces (greater than 2 cm by 4 cm) to be examined and therefore a better sampling of these coarse-grained (3–8 mm) specimens. The whole procedure (pattern acquisition, image freezing, band detection, indexing and result backup) was carried out on the studied sample manually due to coarse grain size and chemical alteration at grain boundaries. Thus, each individual grain is represented by only one orientation measurement. As previously mentioned, the grain size is

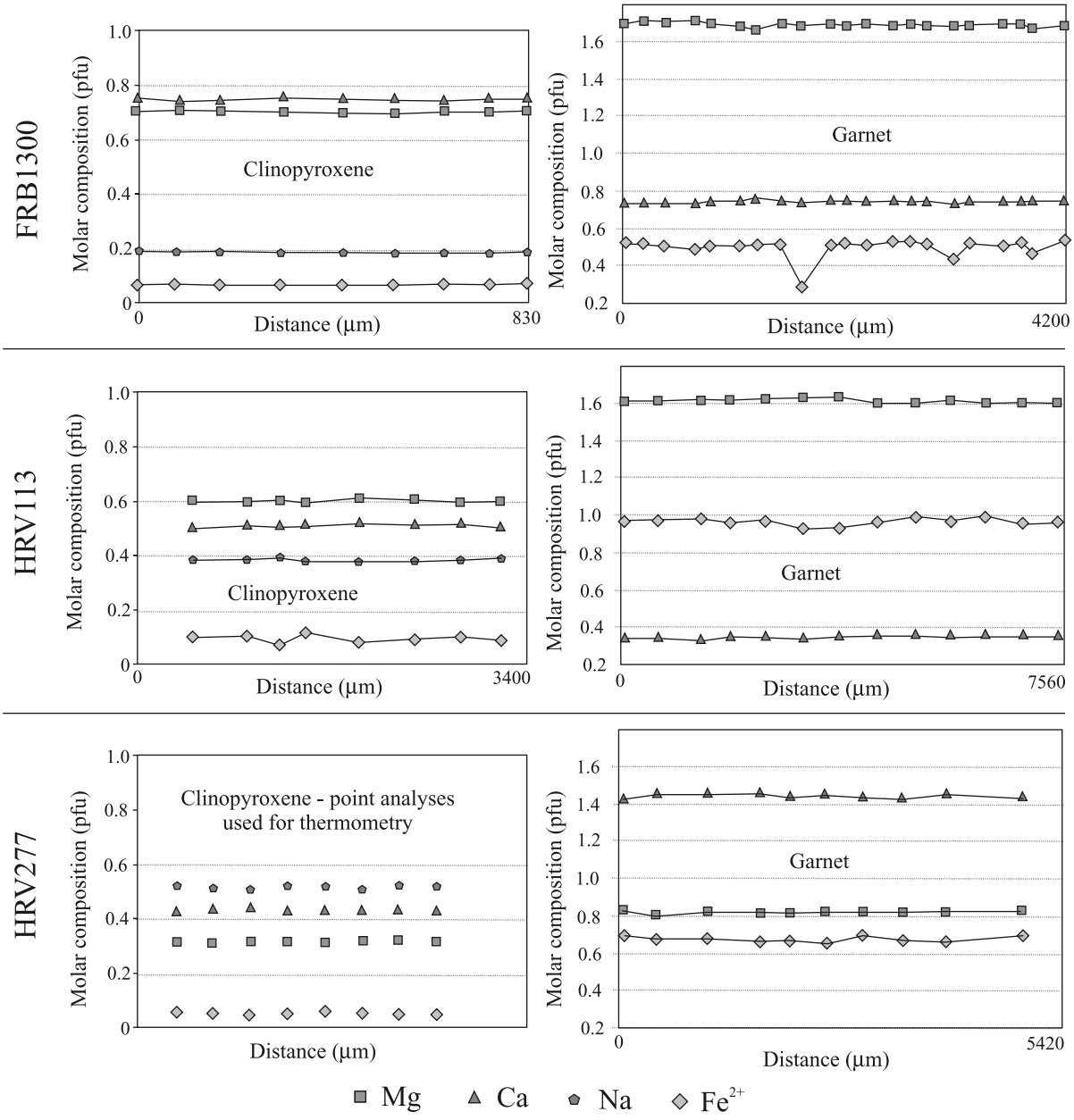

Fig. 2. Results of microprobe point analysis profiling through clinopyroxenes and garnets in all three samples. Plots show relative distance between individual points of analysis versus amount of Mg, Ca, Na and Fe^{2+} per formula unit.

coarse, but the grain size distribution is narrow and monomodal, hence we give equal weighting to each orientation measurement for the contouring pole figures.

Clinopyroxene LPO was measured from thin sections cut parallel to elongation of garnet grains and perpendicular to alternation of clinopyroxene and garnet rich bands. The measured LPO of clinopyroxene is presented on non-polar, lower hemisphere equal area projections in the structural (XZ) reference frame defined by grain shape; thus, trace of the foliation is horizontal with lineation (X) in the conventional East–West direction. Note the geographical notation has no significance in this case, as the xenoliths are not orientated in the field. The LPO is illustrated by four pole figures of [100], [001], (010) and (110), respectively, the main slip directions and planes for clinopyroxenes.

3.3. Numerical simulation of LPO

Lattice preferred orientations were predicted using an anisotropic visco-plastic self-consistent model (VPSC). The background of the model and its application to clinopyroxene have been described in detail by Bascou et al. (2002), thus only a short overview is presented in the following section. The visco-plastic self-consistent approach allows both the microscopic stress and strain rate to differ from the corresponding macroscopic

quantities. Strain compatibility and stress equilibrium are ensured at the aggregate scale. At the grain scale, deformation is accommodated by dislocation glide only; other mechanisms such as dynamic recrystallization and grain boundary sliding are not taken into account. The shear strain rate in a slip system s is related to the local deviatoric stress tensor $\mathbf{s}$ by a visco-plastic law:

$$\dot{\gamma}^s = \dot{\gamma}_0 \left(\frac{\tau^s_r}{\tau^s_0} \right)^{n^s} = \dot{\gamma}_0 \left(\frac{r^s_r s_{ij}}{\tau^s_0} \right)^{n^s} \quad (1)$$

where $\dot{\gamma}_0$ is a reference strain rate and n^s, τ^s_r, τ^s_0 and are, respectively, the stress exponent, the resolved shear stress, and the critical resolved shear stress for the system s, whose orientation relative to the macroscopic stress axes is expressed by its Schmid tensor $\mathbf{r}^s$. The potentially active slip systems for clinopyroxene, their critical resolved shear stresses, and their stress exponents (Table 1) are evaluated from microscopic studies of naturally and experimentally deformed eclogites and from single-crystal diopside deformation experiments as summarized by Bascou et al. (2002).

The problem lies in the calculation of a microscopic state ($\mathbf{s}$, $\dot{\varepsilon}$) for each grain, whose volume average determines the response of the polycrystal ($\bar{\Sigma}$, $\bar{\mathbf{D}}$). The '1-site' approximation (Molinari et al., 1987) is used in the anisotropic VPSC formulation; the influence of neighboring grains is not taken into account. Interactions between any individual grain and its surroundings are successively replaced by the interaction between an inclusion with similar lattice orientation and an infinite homogeneous equivalent medium (HEM), whose behavior is the weighted average of the behavior of all the other grains. This leads to:

$$\dot{\varepsilon}_{ij} - D_{ij} = -\alpha \tilde{\mathbf{M}}_{ijkl} \left(s_{kl} - \bar{\Sigma}_{kl} \right) \quad (2)$$

where $\tilde{\mathbf{M}}$ is the interaction tensor and α is a constant used to parameterize the interaction between grains and the HEM. $\alpha = 0$ corresponds to the upper bound homogeneous strain (Taylor) model (Lebensohn and Tomé, 1993), $\alpha = 1$ corresponds to the tangent model of Lebensohn and Tomé (1993), and $\alpha =$ infinity to the lower bound stress equilibrium model (Chastel et al., 1993). The study by Bascou et al. (2002) demonstrated that the VPSC tangent model ($\alpha = 1$) reproduced all the main features of the LPO of naturally deformed omphacite and has been applied here.

In the models an aggregate of 1000 clinopyroxene grains, initially spherical in shape and randomly oriented, is deformed in axially symmetric compression, axially symmetric extension, simple shear and pure shear. The strain path is imposed by prescribing a constant macroscopic velocity gradient tensor $\mathbf{L}$, for axially symmetric compression, axially symmetric extension, simple shear, and pure shear and a time increment, dt, set to achieve an equivalent strain of 0.025 in each deformation step. The equivalent strain is defined as (Molinari et al., 1987):

$$\varepsilon_{eq} = \int D_{eq}(t) \mathrm{d}t \quad (3)$$

where the Von Mises equivalent strain rate is:

$$\mathbf{D}_{eq} = \sqrt{2/3 \mathbf{D}_{ij} \mathbf{D}_{ij}} \quad (4)$$

The velocity gradient tensors for axially symmetric compression ($\mathbf{L}_{AC}$), axially symmetric extension ($\mathbf{L}_{AE}$), simple shear ($\mathbf{L}_{SS}$), and pure shear ($\mathbf{L}_{PS}$) are given by:

$$\mathbf{L}_{AC} = \begin{bmatrix} 0.5 & 0 & 0 \\ 0 & -1 & 0 \\ 0 & 0 & 0.5 \end{bmatrix}, \quad \mathbf{L}_{AE} = \begin{bmatrix} -0.5 & 0 & 0 \\ 0 & 1 & 0 \\ 0 & 0 & -0.5 \end{bmatrix},$$

$$\mathbf{L}_{SS} = \begin{bmatrix} 0 & 1 & 0 \\ 0 & 0 & 0 \\ 0 & 0 & 0 \end{bmatrix}, \quad \mathbf{L}_{PS} = \begin{bmatrix} 1 & 0 & 0 \\ 0 & -1 & 0 \\ 0 & 0 & 0 \end{bmatrix} \quad (5)$$

The main objective of the VPSC modeling to assessment of the influence of $\langle 110 \rangle \{ 1\bar{1}0 \}$ slip systems on development of either S- or L-type of LPO of clinopyroxene, which was the main argument for the cation ordering model (Brenker et al., 2002). Therefore VPSC model calculations for each deformation regime has been carried out using two end-member values of CRSS for $\langle 110 \rangle \{ 1\bar{1}0 \}$, in order to simulate either high activity of this slip system (CRSS = 1) or very low activity of the slip system (CRSS = 10).

Table 1
Families of slip systems used in the CRSS models. Critical resolved shear stresses are normalized by the CRSS of the [001](100) slip system

Slip system	CRSS
[001](100)	1
[001](110) [001](1$\bar{1}$0)	10
[1$\bar{1}$0](110) [110](1$\bar{1}$0)	1 or 10
[100](010)	3
[001](010)	8
[1$\bar{1}$2](110) [112](1$\bar{1}$0) [1$\bar{1}$2](110) [1$\bar{1}$2](1$\bar{1}$0)	10
[010](100)	10
[101](010)	10

3.4. Eigenvalue analysis of (010) and [001] pole figure symmetry

Some authors have tried to give more precise descriptions of the end-member L-type, a mixture of L and S called LS, or end-member S-type by using the eigenvalue classification proposed for field data by Vollmer (1990) and previously used for the LPO of omphacite by Ábalos (1997) and Mauler et al. (2001). In this approach, first one calculates the normalized orientation tensor ($\mathbf{M}_{jk}$) defined here as:

$$\mathbf{M}_{jk} = \frac{1}{N}\begin{bmatrix} \sum_i^N x_i^2 & \sum_i^N x_i y_i & \sum_i^N x_i z_i \\ \sum_i^N x_i y_i & \sum_i^N y_i^2 & \sum_i^N y_i z_i \\ \sum_i^N x_i z_i & \sum_i^N y_i z_i & \sum_i^N z_i^2 \end{bmatrix} \quad (6)$$

where x_i, y_i and z_i are the three direction cosines of the ith crystallographic direction (e.g. pole to (010) or [001] direction) in XYZ Cartesian sample coordinates defined by the micro-structural frame for the naturally deformed samples and principal finite strain axes for the VPSC models. The eigenvalues and eigenvectors of the symmetric matrix $\mathbf{M}_{jk}$ were determined by Jacobi iteration. The orientation of the eigenvectors has been plotted on all (010) and [001] pole figures. The magnitude of three eigenvalues ($\lambda_1 \geqq \lambda_2 \geqq \lambda_3$ with the normalization $\lambda_1+\lambda_2+\lambda_3=1$) are used to define three fabric indices proposed by Vollmer (1990), point maximum ($P=\lambda_1-\lambda_2$; P has a high value when $\lambda_1 > \lambda_2 \approx \lambda_3$), girdle ($G=2(\lambda_2-\lambda_3)$; G has a high value when $\lambda_1 \approx \lambda_2 > \lambda_3$) and random ($R=3\lambda_3$; R has a high value when $\lambda_1 \approx \lambda_2 \approx \lambda_3$). These indices range from zero to one and have the property that $P+G+R=1$. The eigenvalue analysis only applies to one pole figure. To determine, in a more objective manner, if the omphacite LPO is S-type or L-type we need to combine the eigenvalue analyses of the (010) and [001] pole figures. We know that the (010) pole figure for the end-member L-type should have a perfect girdle fabric, hence $P=0$, $G=1$ and $R=0$ and for the end-member S-type fabric should have a perfect point maximum, hence $P=1$, $G=0$ and $R=0$. Similarly, for [001] pole figure for the end-member L-type should have a perfect point maximum fabric, hence $P=1$, $G=0$ and $R=0$ and for the end-member S-type fabric should have a perfect girdle, hence $P=0$, $G=1$ and $R=0$. We introduce the LS index, which has a value of one for the end-member L-type and a value of zero for the end-member S-type omphacite fabric, which is defined as:

$$\mathrm{LS}_{\mathrm{index}} = \frac{1}{2}\left[2 - \left(\frac{P_{010}}{G_{010}+P_{010}}\right) - \left(\frac{G_{001}}{G_{001}+P_{001}}\right)\right] \quad (7)$$

where the subscripts of the P and G indices refer to the pole figures (010) or [001]. Note that for real data, the random index R is never zero, hence the P_{010} and G_{001} values are normalized by the sum of $G_{010}+P_{010}$ and $G_{001}+P_{001}$, respectively, to give the desired range of 0–1 for any value of R.

4. Results

4.1. Chemical analysis and equilibration temperature

Generally, microprobe analysis profiling demonstrated the chemical homogeneity of both principal minerals; however, samples have different chemical composition (Fig. 2). Sample FRB1300 showed Mg-rich/Fe-poor garnet composition indicating enrichment in pyrope and a higher content of grossular than almandine component. Clinopyroxenes in the same sample are dominantly diopsidic in composition. Sample HRV113 has garnet rich in pyrope, but a considerably higher content of almandine than grossular component. Clinopyroxenes in this sample have a higher content of jadeite and less diopside. Average content of K_2O_{cpx} and Na_2O_{grt} in both samples are characteristic of Group I eclogites formed under conditions similar to those required for diamond genesis ($P>4.5$ GPa). Temperatures estimated for sample FRB1300 are higher (1088–1116 °C) than sample HRV113 (962–991 °C) (see Table 2).

A xenolith of the same composition as HRV277 has been already the subject of a detailed petrological study because of its exceptional mineral assemblage, with a first report of coesite from a non-impact environment by Smyth and Hatton (1977). They determined the unit cell of K–feldspar, which is consistent with sanidine in a very high degree of Al–Si disorder indicating equilibration above 900 °C and 3.0 GPa. Their clinopyroxene analyses revealed an enrichment in the Ca–tschermak component and an amount of Al^{VI} in excess of $Na+K+Al^{IV}$ indicating a significant apparent charge imbalance or cation vacancy concentration in the pyroxene which can only be stable at high pressures. Our microprobe analysis of the sample HRV277 demonstrates the homogeneous composition of garnet enriched in the grossular component (X_{Grs} in grt = 0.458). Clinopyroxenes are strongly altered with isolated areas of the original composition, thus a profile of the composition across the crystal of clinopyroxene was not undertaken. In order to obtain the original chemistry for the estimation of equilibration temperatures, the concentration of principal cations were measured at eight small regions of unaltered clinopyroxene; the analyses are shown in Fig. 2 (bottom left). The original composition shows a high content of jadeite (X_{Jd} in cpx = 0.52), which is the highest value of the three samples. Sample HRV277 also shows the highest temperatures of equilibration between 1130 and 1145 °C (Table 2). The average contents of K_2O_{cpx} and Na_2O_{grt} show that the samples belong to the Group I eclogites equilibrated at pressures higher than 4.5 GPa.

4.2. Lattice preferred orientation

Generally, omphacite LPO shows a strong concentration of [001] axes parallel to lineation and (010) poles in a plane normal to lineation forming a girdle with a maximum at a high angle to the foliation (Fig. 3). The [100] axes show no systematic pattern, but a maximum is always present in a plane normal to lineation. The (110) poles form in a weak girdle perpendicular to the lineation with a weak maximum near the normal to the foliation (Z). Presented LPOs of omphacite can be interpreted as preferred orientations suited for easy slip on

Table 2
Typical point microprobe analyses of the clinopyroxene and garnet for samples FRB1300, HRV113 and HRV277. Average Na_2O_{grt} (wt%), K_2O_{cpx} (wt%), X_{Jd} in cpx and calculated temperatures using the geothermometers of Ai (1994), Powell (1985) and Ellis and Green (1979)

	FRB1300		HRV113		HRV277	
Oxide	cpx	Garnet	cpx	Garnet	cpx	Garnet
SiO_2	54.31	41.25	55.59	41.25	55.73	39.64
TiO_2	0.19	0.15	0.4	0.33	0.12	0.14
Cr_2O_3	0.17	0.19	0.12	0.17	0.09	0.06
Al_2O_3	7.35	23.98	8.08	22.44	17.16	22.44
Fe_2O_3	0	0.96	1.66	0	0	1.75
FeO	2.19	8.37	3.53	16.1	1.6	10.54
MnO	0.03	0.27	0.17	0.55	0	0.37
MgO	13.2	15.82	11.26	14.65	6.04	7.43
CaO	19.4	9.67	13.3	4.34	11.23	17.95
Na_2O	2.63	0.05	5.52	0.14	7.55	0.08
K_2O	0.14	0.01	0.14	0	0.19	0
Total	99.61	100.72	99.77	99.97	99.71	100.4
Av. Na_2O_{grt} (wt%)		0.045		0.12		0.075
Av. K_2O_{cpx} (wt%)		0.125		0.14		0.19
X_{Prp}–X_{Alm}–X_{Grs} in grt		0.57–0.17–0.20		0.54–0.32–0.07		0.28–0.23–0.45
X_{Jd}–X_{Di} in cpx		0.19–0.66		0.32–0.40		0.52–0.36
Ellis and Green (1979)		1116 °C		991 °C		1145 °C
Powell (1985)		1103 °C		969 °C		1138 °C
Ai (1994)		1088 °C		962 °C		1129 °C

(110) and (010) slip planes with a common slip direction [001], assuming that plastic deformation occurred by regime close to simple or pure shear with the extension direction near X and pole to the flattening plane near Z.

Besides the general features, variations of LPO are observed. In samples HRV277 and FRB1300 the foliation planes are well defined by the elongation of garnet grains. In sample FRB1300, but not in HVR277, there is a slight obliquity of the [001] axes maximum from the direction of lineation and inclination of girdles of (010) and (110) planes from the position normal to the lineation. In sample HRV113 we cannot comment on the slight obliquity of the [001] axes maximum from the direction of lineation as the foliation is not well defined and it may simply represent an error in the determination of the foliation plane. LPO of all three measured samples have a strong concentration of [001] axes close to the lineation, typical of the L-type. The distribution of the (010) poles has some characteristics of the L-type with girdle normal to the lineation, but also has some characteristics of S-type with a high concentration of (010) at a high angle to the foliation.

4.3. Numerical simulation of LPO

Changing the CRSS of the $\langle 110\rangle\{1\bar{1}0\}$ slip systems by one order of magnitude has almost no influence on final LPO of clinopyroxene (Figs. 4 and 5) at an equivalent strain of one. In axially symmetric compression and extension the two end-member LPO types are produced. In axially symmetric compression the end-member S-type pattern develops with the (010) pole figure with a strong point maximum parallel to the compression axis Z, whereas [001] has developed a strong girdle in the finite strain flattening (XY) plane. Apart from some differences in the distribution of [100] axes the patterns are very similar for CRSS = 1 and CRSS = 10 simulations. The pole figures of CRSS = 10 simulations tend to have a higher maximum densities than for CRSS = 1. In axially symmetric extension the end-member L-type pattern develops with the (010) pole figure with girdle normal to the extension axis X, whereas [001] has developed a strong point maximum parallel to the extension axis X. The patterns and densities in the pole figures is very similar for the CRSS = 1 and CRSS = 10 VPSC models. The distribution patterns and densities are very similar for all pole figures for the two models with CRSS = 1 and CRSS = 10 in both plane strain deformation modes (Fig. 5). The (010) and [001] pole figures have characteristics of both the L- and S-types and can be classified as a LS-type. The (010) pole figure illustrates better this LS-type with a girdle normal to the X-axis and a high concentration of pole parallel to the Z-axis. Again it is the [100] pole figure where the most noticeable differences in distribution are seen between the CRSS = 1 and CRSS = 10 models.

The slip activity for the dominant slip systems for all the deformation regimes are present in Table 3 for an equivalent strain of one, the same strain level as for the pole figures in Figs. 4 and 5. Changing the CRSS of $\langle 110\rangle\{1\bar{1}0\}$ slip system from 1 to 10 results in a reduction of the activity on this system by 80%. The reduction of the activity on the $\langle 110\rangle\{1\bar{1}0\}$ slip system is compensated by an increased activity on the [100](010) and [001](010) slip systems by

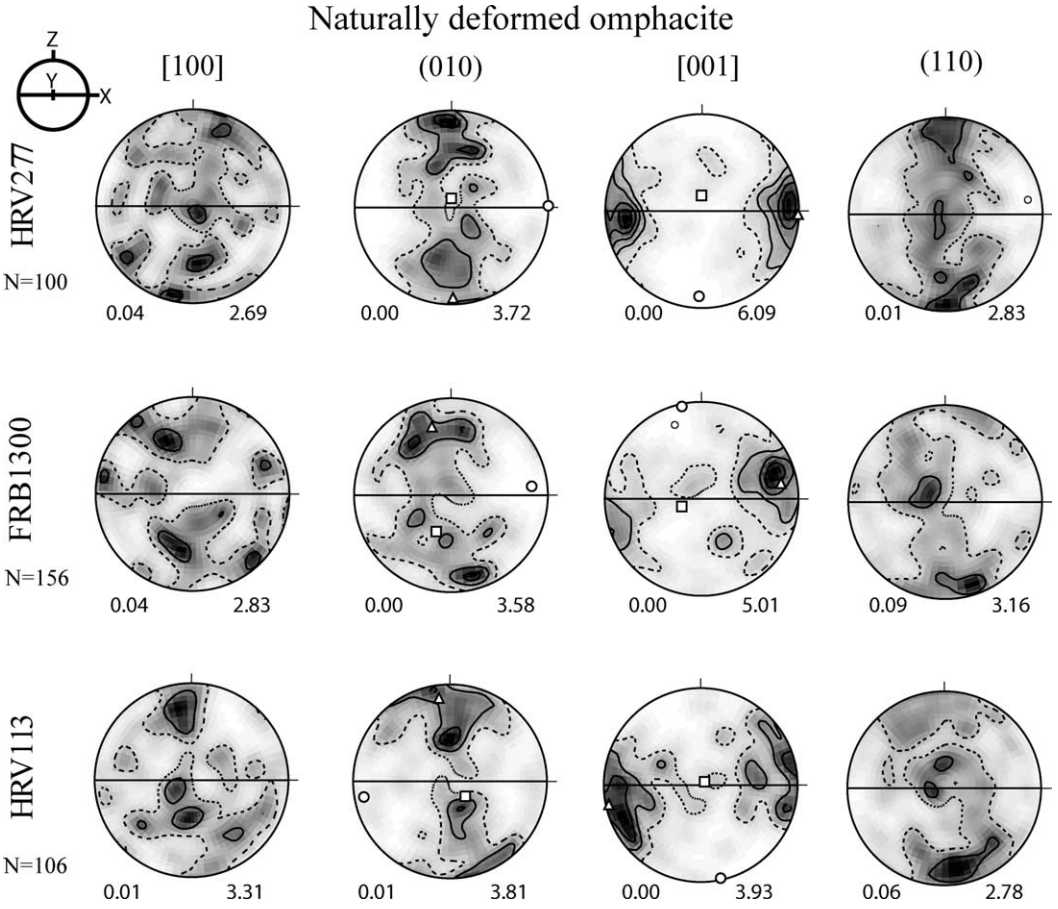

Fig. 3. Omphacite LPO measure using the EBSD technique. Equal area projection, lower hemisphere. Contoured at interval 1.0 times of uniform distribution. Foliation (full line) is horizontal and lineation is in this plane in E–W direction. *N* is the number of measured grains. Minimum and maximum densities are marked on the bottom left and right, respectively, of each pole figure. The position of maximum, intermediate and minimum eigenvalues are marked on the (010) and [001] pole figures by white triangle, square and circle, respectively.

approximately two and three times, respectively. The slip activity on the [001](100) is not greatly affected by the changes in activity occurring on the $\langle 110\rangle\{1\bar{1}0\}$ slip system. The [001](100) slip system is the most active for all deformation regimes except axially symmetric compression when CRSS of $\langle 110\rangle\{1\bar{1}0\}$ is equal to 10. In no case investigated did the LPO type change from S- to L-type when the activity of the $\langle 110\rangle\{1\bar{1}0\}$ system was reduced by 80%. Additional VPSC models with no activity of the $\langle 110\rangle\{1\bar{1}0\}$ system (CRSS $= \infty$) give identical results to the CRSS $= 10$ simulations for the pole figures.

4.4. Eigenvalue analysis of (010) and [001] pole figure symmetry

The values of all indices given in Table 4 show that the three naturally deformed samples have $P > G$ for the [001] pole figure and $G > P$ for (010) pole figures The P and G

Table 3
Slip system activities. AC, AE, SS and PS are, respectively, the axially symmetric compression, axially symmetric extension, simple shear and pure shear VPSC models at an equivalent strain of one. 1 and 10 indicate the value of CRSS for the $\langle\bar{1}10\rangle\{110\}$ slip system used in the VPSC model. Activities in percent of total slip activity

Deformation regime	[001](100)	[100](010)	[001](010)	$\langle\bar{1}10\rangle\{110\}$
AC1	26.00	12.20	3.47	54.00
AC10	16.70	26.10	9.70	16.01
AE1	59.70	2.76	5.76	27.50
AE10	65.90	6.08	10.30	4.17
SS1	39.00	13.10	4.60	39.00
SS10	39.60	20.90	12.30	6.81
PS1	48.00	7.02	4.11	37.10
PS10	43.80	15.80	11.60	7.91

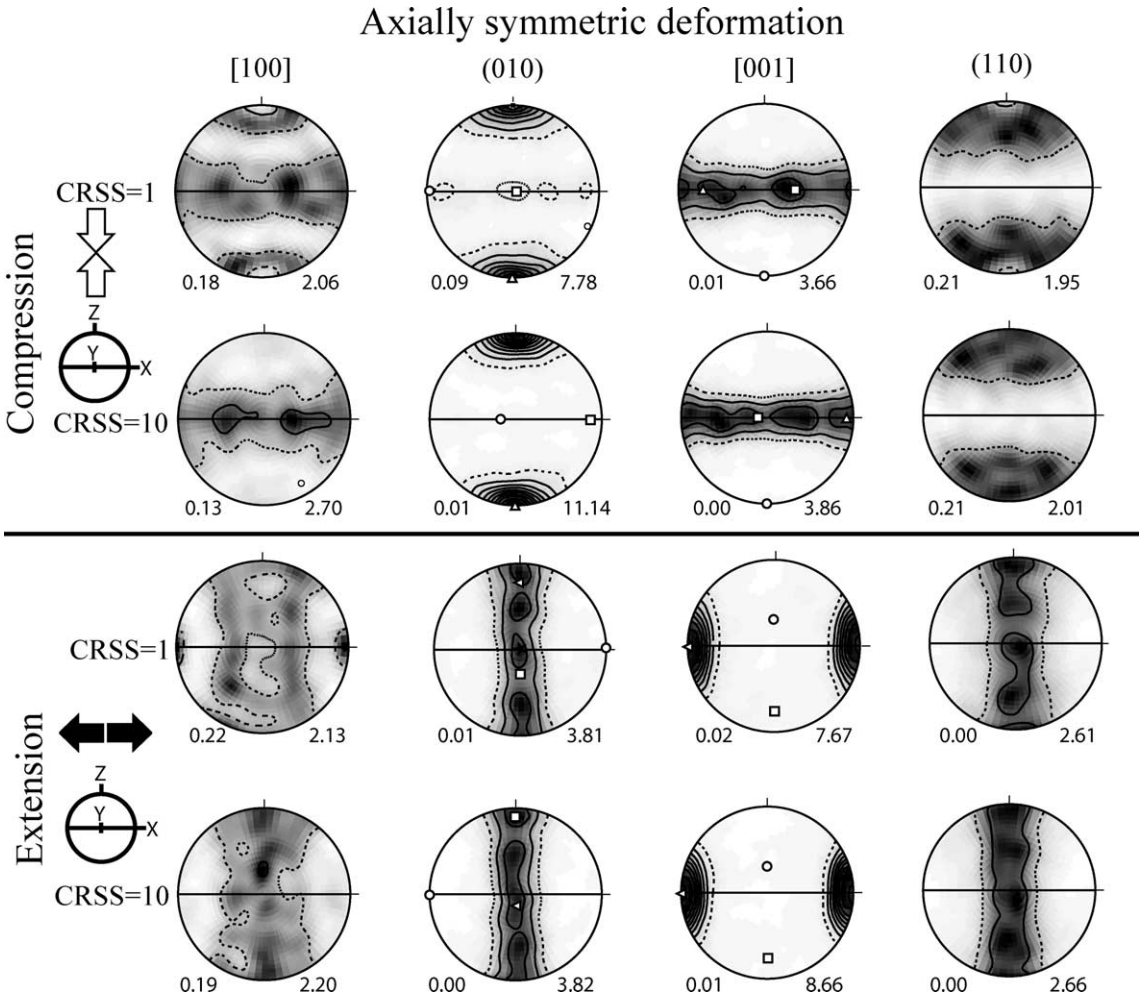

Fig. 4. Clinopyroxene LPO simulated in VPSC model with $\alpha = 1$ and CRSS values of 1 or 10 for assessed $\langle 110\rangle\{1\bar{1}0\}$ slip systems at an equivalent strain of one for axially symmetric compression and extension. Equal area projections, lower hemisphere. Full line (XY plane) is horizontal, compression direction is parallel to Z (white vertical arrows) and extension direction is parallel to X (black horizontal arrows). Minimum and maximum densities are marked on the bottom left and right, respectively, of each pole figure. The position of maximum, intermediate and minimum eigenvalues are marked on the (010) and [001] pole figures by white triangle, square and circle, respectively.

values confirm that the fabrics are of LS type with a stronger L character than S. In all samples the R index is greater than either the P or G, suggesting that the orientations have a high random component, which is not confirmed by the pole figures, particularly the [001] pole figures. The LS index has a value between 0.61 and 0.85, indicating that these naturally deformed samples are much closer to the L-type end-member than S-type end-member.

We have also calculated all the fabric indices for the VPSC simulations and results for an equivalent strain of one are given in Table 4. In general the VPSC model [001] and (010) pole figures have a much lower R index than the naturally deformed samples, with the possible exception of the axially symmetric compression models. As expected the axially symmetric compression models have very high values of G for [001] pole figures and P for (010) pole figures. The LS index confirms the result with a value very close to zero, characteristic of the S-type end-member. The difference between the models for CRSS for the $\langle\bar{1}10\rangle\{110\}$ slip system at 1 and 10 is very small for the P, G and R indices of [001] pole figures and the LS index, the differences are more important for (010) pole figures. For the axially symmetric extension models the values are very high for P for [001] pole figures and G for (010) pole figures. The LS index has a value very close to one, characteristic of the L-type end-member. The differences between the models for CRSS for the $\langle\bar{1}10\rangle$ $\{110\}$ slip system at 1 and 10 is very small for all indices, this is also true for all the other models, with the exception of the axially symmetric compression just mentioned above. In the simple shear and pure shear models the characteristics are very similar with P and G indices having similar values, but with $P_{001} > G_{001}$ and $P_{010} < G_{010}$ resulting in a LS index between 0.55 and 0.63, characteristic of mixed LS-type fabric. We have also plotted the evolution of the LS index as a function of equivalent strain for all deformation modes (Fig. 6). The LS

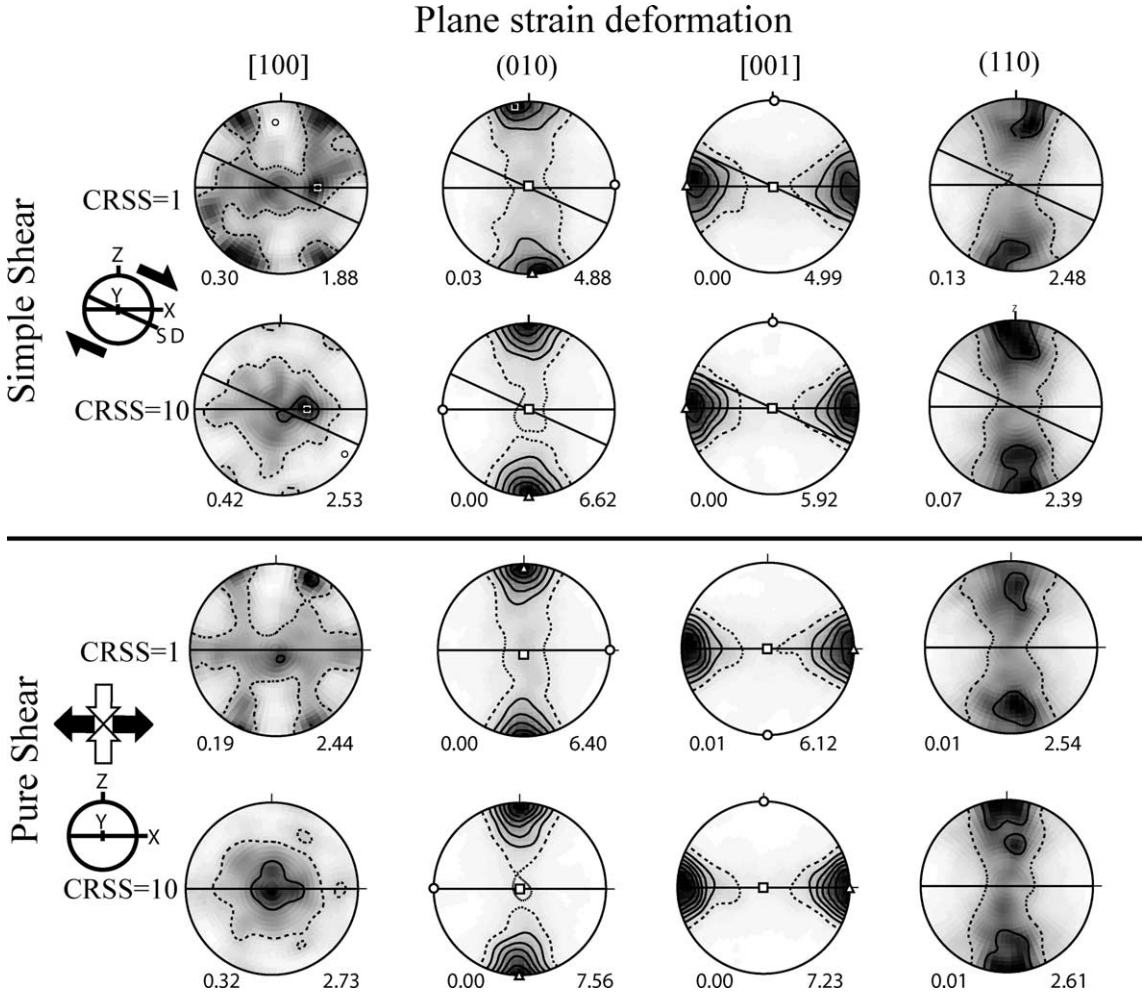

Fig. 5. Clinopyroxene LPO simulated in VPSC model with $\alpha = 1$ and CRSS values of 1 or 10 for assessed $\langle 110\rangle\{1\bar{1}0\}$ slip systems at an equivalent strain of one for simple shear and pure shear. Equal area projections, lower hemisphere. Full line (XY plane) is horizontal. In simple shear the inclined black line marks the shear plane, the direction of shear is indicated by SD, and the shear sense is marked by black arrows. In pure shear the compression direction is parallel to Z (white vertical arrows) and extension direction is parallel to X (black horizontal arrows). Minimum and maximum densities are marked on the bottom left and right, respectively, of each pole figure. The position of maximum, intermediate and minimum eigenvalues are marked on the (010) and [001] pole figures by white triangle, square and circle, respectively.

Table 4
Eigenvalue analyses of the [001] and (010) pole figures. P = point, G = girdle and R = random are fabric indices defined by the eigenvalues of the [001] and (010) pole figures, section on the LS index is combined index of the [001] and (010) pole figures which is defined in the text, which is equal to one for a perfect L-type and equal to zero for a perfect S-type omphacite LPO based on the [001] and (010) pole figures. AC AE, SS and PS are, respectively, the LPO corresponding to axially symmetric compression, axially symmetric extension, simple shear and pure shear VPSC models for a equivalent strain of one. 1 and 10 indicate the value of CRSS for the $\langle\bar{1}10\rangle\{110\}$ slip system used in the VPSC model

Sample	P_{001}	G_{001}	R_{001}	P_{010}	G_{010}	R_{010}	LS index
HRV277	0.47	0.12	0.40	0.06	0.56	0.37	0.85
FRB1300	0.29	0.11	0.60	0.04	0.46	0.50	0.82
HRV113	0.30	0.26	0.44	0.15	0.32	0.53	0.61
AC1	0.00	0.82	0.18	0.38	0.02	0.61	0.02
AC10	0.01	0.86	0.12	0.64	0.01	0.36	0.01
AE1	0.65	0.00	0.35	0.02	0.80	0.18	0.99
AE10	0.72	0.01	0.27	0.01	0.86	0.13	0.99
SS1	0.37	0.38	0.26	0.19	0.44	0.36	0.60
SS10	0.46	0.36	0.18	0.35	0.42	0.23	0.55
PS1	0.44	0.35	0.20	0.23	0.53	0.25	0.63
PS10	0.52	0.34	0.15	0.41	0.42	0.18	0.55

index is perfectly constant for axially symmetric deformation after an equivalent strain of 0.4 and nearly constant for simple and pure shear.

5. Discussion

Several observations have been put forward by Brenker et al. (2002) for the cation ordering control of the development of S- and L-type LPOs of omphacite. The first observation for the cation-ordering model is the position of the fabric type on the phase diagram of omphacite in the jadeite content versus temperature coordinates (fig. 7 of Brenker et al., 2002) plotting their own LPO data with data from Ábalos (1997) and Godard and Van Roermund (1995). Their resulting plot has been presented as a strong correlation between LPO type and ordering state of omphacite. The three mantle eclogites that came up to the surface as xenoliths in kimberlite pipes contain omphacites with an essentially L- or LS-type LPO (Table 4) with LS-index between 0.61 and 0.85. The jadeite content in clinopyroxene and calculated equilibrium temperatures (950–1150 °C) suggest the presence of a completely disordered structure of omphacite (Fig. 7). Thus our data do not show any correlation with the proposed structural control of Brenker et al. (2002) as they occur deep inside the suggested S-type LPO region associated with disordered omphacite of C2/c space group. Additional indications that correlation between cation ordering and LPO type is very poor can be found in the work of Kurz et al. (2004), which presented contrasting textures (from

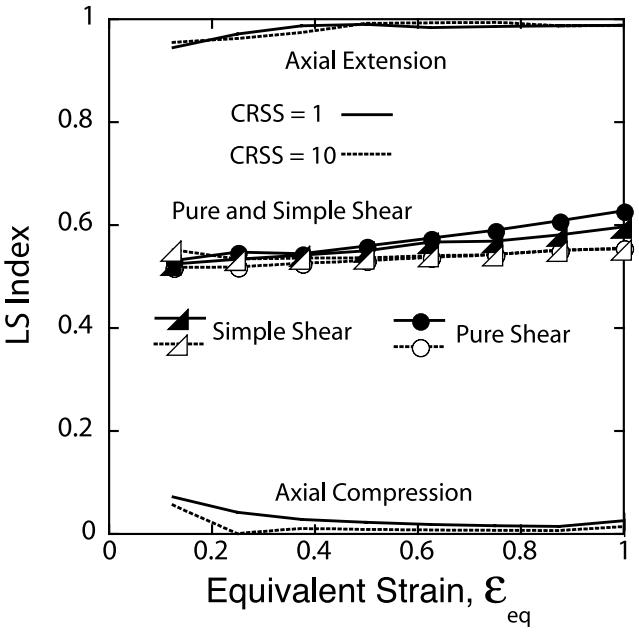

Fig. 6. Evolution of the LS-index with progressively increasing equivalent strain in the VPSC models with $\alpha = 1$ and CRSS values of 1 or 10 for assessed $\langle 110\rangle\{1\bar{1}0\}$ slip systems for axially symmetric compression and axially symmetric extension, simple shear and pure shear. Solid black line for CRSS = 1 and dashed black line for CRSS = 10 for the $\langle 110\rangle\{1\bar{1}0\}$ slip systems.

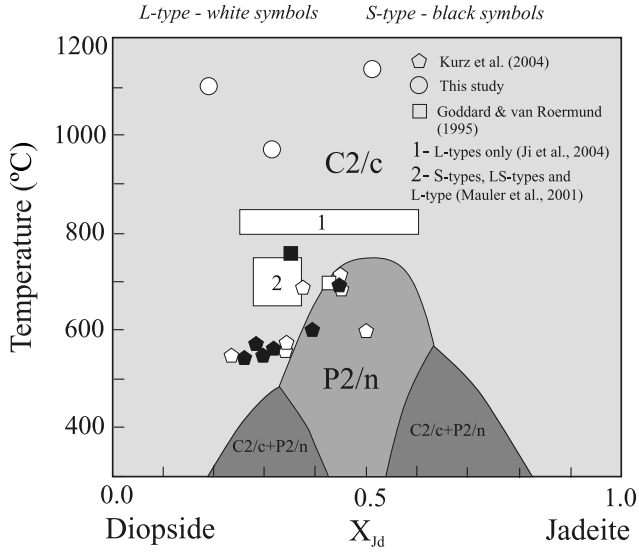

Fig. 7. Equilibrium phase diagram of omphacite show occurrence of C2/c and P2/n space groups as a function of jadeite content (X_{Jd}) and deformation temperature. Plotted data from this work and previous studies show that there is no correlation between space group type and lattice preferred orientation type as was proposed by Brenker (1998).

L- to S-type LPOs) formed at approximately the same PT conditions and nearly the same omphacite composition (Kurz et al., 2004) (Fig. 7).

The ordering state of clinopyroxenes in our samples was not verified by a TEM study; however, there are several arguments for their completely disordered structure that will be presented. Experiments on the kinetic behavior of cation ordering in omphacites show that at a temperature of 1000 °C, the structure is nearly completely disordered within 20 h (Carpenter et al., 1990). A similar experiment at a higher pressure of 1.8 GPa showed even higher rates of disordering (Carpenter, 1981). Hence at mantle PT conditions omphacite will be completely disordered. This is also supported by study of the ordering state of clinopyroxenes in eclogite xenoliths from the Roberts Victor mine, near Kimberley, South Africa (Kushiro and Aoki, 1968; Yokoyama et al., 1976), the same location as our samples, which showed a fully disordered structure. A change of ordering state of the samples during exhumation and cooling seems unlikely. Study of the thermal history of ascending xenoliths in kimberlitic magma from the Premier mine and Tsaba Putsoa show that their temperature can even increase depending on the diameter of xenolith during their rapid ascent (Mercier, 1979). Velocities of ascent based on kinetics of neoblasts growth in xenoliths range between 40 and 70 km/h^{-1} (Mercier, 1979), which means that xenoliths cover the whole distance from the sampling site to the surface within a few hours and must be quenched preserving the original structure of the minerals at mantle conditions. Significant plastic deformation required to produce an LPO during the rapid ascent is incompatible with the high temperature low stress microstructure of the nodules.

From the microstructural point of view, the cation ordering model is based on TEM observation of dissociated dislocations with $\mathbf{b}=1/2\langle\bar{1}10\rangle$ separated by a stacking fault in the P2/n structure of omphacite, which would have to constrict and form unit dislocation in order to climb or cross-slip. In contrast, the same dislocation in the C2/c structure is not dissociated, and hence climb or cross-slip should be relatively easy. Consequently, easily gliding $1/2\langle110\rangle\{1\bar{1}0\}$ slip system in the C2/c structure together with [001](100) and [001](110) give rise to the S-type LPO according to Brenker et al. (2002).

Although a defect structure almost certainly exists on the cation sublattice in the ordered structure, there is no direct evidence to support that this has strong implications for dislocation mobility, as it is more likely that strong Si–O bonds associated with silicon tetrahedra exercise a greater control on mobility than cation distribution. From the VPSC models we can show that changing the CRSS by one order of magnitude for a $\langle110\rangle\{1\bar{1}0\}$ slip system results in the activity of the system being reduced by 80%. Despite this drastic change from $\langle110\rangle\{1\bar{1}0\}$ being the dominant slip system to one with about 10% of the total slip activity, almost no change in the fabric symmetry was observed (Figs. 4 and 5), as shown quantitatively by the LS index (Fig. 6 and Table 4). The VPSC models show that major changes in the activity of the $\langle110\rangle\{1\bar{1}0\}$ slip system cannot be the principal factor controlling the changes in symmetry of LPO development in omphacite from S- to L-type. The major control of fabric symmetry of omphacite deforming by dislocation glide is clearly demonstrated to be the strain path imposed by prescribing a constant macroscopic velocity gradient tensor $\mathbf{L}$ in the VPSC models. A similar conclusion was also reached for the study of the influence of the strain path of quartzites using the Taylor–Bishop–Hill model by Lister and Hobbs (1980). Pervious workers (e.g. Ábalos, 1997; Mauler et al., 2001) have also indicated that S- and L-type LPOs of omphacite have been correlated with macroscopic sample strain symmetry and microscopic shape fabric of clinopyroxene grains. Mauler et al. (2001) produced counter-examples to the proposed LPO model of Brenker et al. (2002), first published in Brenker (1998).

6. Conclusions

We have measured the LPO of the omphacite in three mantle eclogites from the Roberts Victor mine in South Africa. Our estimated temperatures and pressures for these samples, as well as previous work on samples from the same location, show that omphacite in these samples are in the high temperature disordered (C2/c) structure. The LPO of the omphacite has a clear L- to LS-type pattern with [001] axes parallel to the lineation and [010] axes from a girdle normal to the lineation and a LS-index between 0.61 and 0.85. The samples do not conform to the predictions of Brenker et al. (2002) that cation ordering in omphacite exercises a prime control on LPO and that omphacite with the C2/c structure should have the S-type fabric. To further test their hypothesis we conducted VPSC simulations in which we increased the CRSS of the $1/2\langle110\rangle\{1\bar{1}0\}$ by one order of magnitude, which resulted in 80% reduction of slip activity, but saw no significant variation in LPO symmetry. We conclude that $1/2\langle110\rangle\{1\bar{1}0\}$ has relatively little influence on the LPO development of omphacite; hence, cation ordering in omphacite cannot have prime control on LPO development. In the simulations for axially symmetric deformation the end-member S-type develops in compression (LS index ≈ 0) and the end-member L-type develops in extension (LS index ≈ 1). In plane strain deformation the LS-type develops in simple and pure shear with LS-index between 0.55 and 0.60. The LS-index for the constant strain path of the simulations is nearly constant with increasing strain. According to our VPSC simulations and previously presented simulations by Bascou et al. (2002), the main control on omphacite LPO comes from the activity of [001](100), [100](010) and [001](01) systems combined with the macroscopic strain path.

Acknowledgements

This work has been supported by the Czech GAČR post-doc grant no. 205/03/P065 and the post-doc grant of the French Ministere de la Recherche, which are strongly acknowledged. SU is grateful to the members of the Laboratoire de Tectonophysique in Montpellier and of Mineral Services (Pty) Ltd in Cape Town for the fruitful discussions on the studied subject and mantle composition and dynamics. Special thanks belong to John Gurney, head of the Mineral Services (Pty) Ltd, who kindly provided samples for this study from his outstanding collection of mantle rocks. DM thanks Gilles Canova for introducing him to VPSC modeling without which this contribution would not have been possible. We thank the two JSG reviewers, Luigi Burlini and Karsten Kunze, for the comments on the initial manuscript. In particular, we thank Karsten Kunze for his detailed review and many questions, which lead the authors to develop the LS-index and many other improvements. We thank Andrea Tommasi for useful discussions.

References

Ábalos, B., 1997. Pmphacite febric variations in the Cabo Ortegal eclogite (NW Spain): relationship with strain symmetry during high-pressure deformation. Journal of Structural Geology 19 (5), 621–637.

Adams, B.L., Wright, S.I., Kunze, K., 1993. Orientation imaging: the emergence of a new microscopy. Metallurgical Transactions 24A, 819–831.

Ai, Y., 1994. A revision of the garnet–clinopyroxene Fe2+–Mg exchange geothermometer. Contributions to Mineralogy and Petrology 115, 467–473.

Avé Lallemant, H.G., 1978. Experimental deformation of diopside and websterite. Tectonophysics 48, 1–27.

Bascou, J., Barruol, G., Vauchez, A., Mainprice, D., Egydio-Silva, M., 2001. EBSD-measured lattice-preferred orientations and seismic properties of eclogites. Tectonophysics 342, 61–80.

Bascou, J., Tommasi, A., Mainprice, D., 2002. Plastic deformation and development of clinopyroxene lattice-preferred orientation in eclogites. Journal of Structural Geology 24, 1357–1368.

Brenker, F.E., 1998. Mikrogefügethermochronometrie für Eklogite. PhD thesis, J.W. Goethe Universität, Frankfurt, Germany.

Brenker, F.E., Prior, D.J., Müller, W.F., 2002. Cation ordering in omphacite and effect on deformation mechanism and lattice preferred orientation (LPO). Journal of Structural Geology 24, 1991–2005.

Carpenter, M., 1979. Omphacites from Greece, Turkey and Guatemala: composition limits of cation ordering. American Mineralogist 64, 102–108.

Carpenter, M., 1981. Time–temperature-transformation (TTT) analysis of cation disordering in omphacites. Contributions to Mineralogy and Petrology 78, 433–440.

Carpenter, M., 1983. Microstructures in sodic pyroxenes: implications and applications. Periodico di Mineralogia—Roma 52, 271–301.

Carpenter, M., Domeneghetti, M.-C., Tazzoli, V., 1990. Application of Landau theory to cation ordering in omphacite II: kinetic behaviour. European Journal of Mineralogy 2, 19–28.

Carswell, D.A., Dawson, J.B., Gibb, F.G.F., 1981. Equilibration conditions of upper mantle eclogites: implications for kyanite bearing and diamondiferous varieties. Mineralogical Magazine 44 (333), 79–89.

Chastel, Y.B., Dawson, P.R., Wenk, H.-R., Bennet, K., 1993. Anisotropic convection with implications for the upper mantle. Journal of Geophysical Research 98, 17757–17771.

Davidson, P.M., Burton, B.P., 1987. Order–disorder in omphacitic pyroxenes: a model for coupled substitutions in the point approximation. American Mineralogist 72, 337–344.

Ellis, D.J., Green, D.H., 1979. An experimental study on the effect of Ca upon garnet–clinopyroxene Fe–Mg exchange equilibria. Contributions to Mineralogy and Petrology 71, 13–22.

Godard, G., Van Roermund, H.L.M., 1995. Deformation-induced clinopyroxene from eclogites. Journal of Structural Geology 17, 1425–1443.

Hatton, C.J., Gurney, J.J., 1978. Roberts Victor eclogites and their relation to the mantle, in: Nixon, P.H. (Ed.), Mantle Xenoliths. John Wiley and Sons Ltd, pp. 453–463.

Helmstaedt, H., Anderson, O.L., Gavasci, A.T., 1972. Petrofabric studies of eclogite, spinel–websterite, and spinel–lherzolite xenoliths from kimberlite-bearing breccia pipes in southeastern Utah and northeastern Arizona. Journal of Geophysical Research 77, 4350–4365.

Kennedy, C.S., Kennedy, G.C., 1976. The equilibrium boundary between graphite and diamond. Journal of Geophysical Research 81 (14), 2467–2470.

Kirby, S.H., Christie, J.M., 1977. Mechanical twinning in diopside Ca (Mg, Fe) Si (sub 2) O (sub 6); structural mechanism and associated crystal defects. Physics and Chemistry of Minerals 1 (2), 137–163.

Kirby, S.H., Kronenberg, A.K., 1984. Deformation of clinopyroxenite; evidence for a transition in flow mechanisms and semibrittle behavior. Journal of Geophysical Research B 89 (5), 3177–3192.

Kollé, J.J., Blacic, J.D., 1983. Deformation of single-crystal clinopyroxenes; 2. Dislocation-controlled flow processes in hedenbergite. Journal of Geophysical Research B 88 (3), 2381–2393.

Kurz, K., Jansen, E., Hundenborn, R., Pleuger, J., Schafer, W., Unzog, W., 2004. Microstructures and crystallographic preferred orientations of omphacite in Alpine eclogites: implications for the exhumation of (ultra-) high-pressure units. Journal of Geodynamics 37, 1–55.

Kushiro, I., Aoki, K.-I., 1968. Origin of some eclogite inclusions in kimberlite. American Mineralogist 53, 1347–1367.

Lebensohn, R.A., Tomé, C.N., 1993. A self-consistent anisotropic approach for the simulation of plastic deformation and texture development of polycrystals: application to zirconion alloys. Acta Metallurgica et Materialia 41, 2611–2624.

Lister, G.S., Hobbs, B.E., 1980. The simulation of fabric development during plastic deformation and its application to quartzite: the influence of deformation history. Journal of Structural Geology 2, 355–370.

Mauler, A., Kunze, K., Burg, J.P., Philippot, P., 1998. Identification of EBSD patterns in a monoclinic solid-state solution series: example of omphacite. Materials Science Forum 275, 705–710.

Mauler, A., Burlini, L., Kunze, K., Philippot, P., Burg, J.P., 2000. P-wave anisotropy in eclogites and relationship to the omphacite crystallographic fabric. Physics and Chemistry of the Earth 25, 119–126.

Mauler, A., Godard, G., Kunze, K., 2001. Crystallographic fabrics of omphacite, rutile and quartz in Vendée eclogites (Armorican Massif, France). Consequences for deformation mechanisms and regimes. Tectonophysics 342, 81–112.

McCandless, T.E., Gurney, J.J., 1989. Sodium in garnet and potassium in clinopyroxene: criteria for classifying mantle eclogites, in: Ross, J. (Ed.), Kimberlites and Related Rocks, their Mantle/Crust Setting Diamonds and Diamond Exploration. Proceedings of the 4th International Kimberlite Conference, Perth GSA Special Publication, 14pp. 827–832.

Mercier, J.-C.C., 1979. Peridotite xenoliths and the dynamics of kimberlite intrusion, in: Boyd, F.R., Meyer, H.O.A. (Eds.), The Mantle Sample; Inclusions in Kimberlites and Other Volcanics. Proceedings of the Second International Kimberlite Conference; Volume 2. American Geophysical Union, Washington, D.C., pp. 197–212.

Molinari, A., Canova, G.R., Azhy, S., 1987. A self-consistent approach of the large deformation polycrystal viscoplasticity. Acta Metallurgica 35, 2983–2994.

Pollack, H.N., Chapman, D.S., 1977. On the regional variation of heat flow, geotherms, and lithospheric thickness. Tectonophysics 38 (3–4), 279–296.

Powell, R., 1985. Regression diagnostics and robust regression in geothermometer–geobarometer calibration: the garnet–clinopyroxene geothermometer revisited. Journal of Metamorphic Geology 3, 231–243.

Ratteron, P., Doukhan, N., Jaoul, O., Doukhan, J.C., 1994. High-temperature deformation of diopside IV: predominance of {110} glide above 1000 °C. Physics of the Earth and Planetary Interiors 82, 209–222.

Ryan, C.G., Griffin, W.L., Pearson, N.J., 1996. Garnet geotherms: pressure–temperature data from Cr–pyrope garnet xenocrysts in volcanic rocks. Journal of Geophysical Research 101 (B3), 5611–5625.

Schmidt, N.H., Olesen, N.Ø., 1989. Computer-aided determination of crystal-lattice orientation from electron-channeling patterns in the SEM. Canadian Mineralogist 27, 15–22.

Shirey, S.B., Carlson, R.W., Richardson, S.H., Menzies, A., Gurney, J.J., Pearson, D.G., Harris, J.F., Wiechert, U., 2001. Archean emplacement of eclogitic components into the lithospheric mantle during formation of the Kaapvaal Craton. Journal of Geophysical Research 28 (13), 2509–2512.

Smyth, J.R., Hatton, C.J., 1977. A coesite–sanidine grospydite from the Roberts Victor kimberlite. Earth and Planetary Science Letters 34 (2), 284–290.

Van Roermund, H.L.M., 1983. Petrofabrics and microstructures of omphacites in a high temperature eclogite from the Swedish Caledonides. Bulletin of Mineralogy 106, 709–713.

Van Roermund, H.L.M., Boland, J.N., 1981. The dislocation substructures of naturally deformed omphacites. Tectonophysics 78, 403–418.

Viljoen, K.S., 1999. Physical characteristics and geochemistry of mantle-derived diamonds. Meteoritics and Planetary Science 34 (A116–A116), 1999.

Vollmer, F.W., 1990. An application of eigenvalue methods to structural domain analysis. Geological Society of America Bulletin 102, 786–791.

Yokoyama, K., Banno, S., Matsumoto, T., 1976. Compositional range of P2/n omphacite from the eclogitic rocks of central Shikoku, Japan. Mineralogical Magazine 40, 773–779.